Optics Letters

Mid-infrared frequency combs at 10 GHz

Abijith S. Kowligy,[1,2,*] David R. Carlson,[1] Daniel D. Hickstein,[1] Henry Timmers,[1] Alexander J. Lind,[1,2] Peter G. Schunemann,[3] Scott B. Papp,[1,2] and Scott A. Diddams[1,2]

[1]Time and Frequency Division, National Institute of Standards and Technology, Boulder, Colorado 80305, USA
[2]Department of Physics, University of Colorado, Boulder, Colorado 80309, USA
[3]BAE Systems, Nashua, New Hampshire 03060, USA
*Corresponding author: abijith.kowligy@gmail.com

Received 28 February 2020; revised 19 May 2020; accepted 22 May 2020; posted 26 May 2020 (Doc. ID 391651); published 29 June 2020

We demonstrate mid-infrared (MIR) frequency combs at 10 GHz repetition rate via intra-pulse difference-frequency generation (DFG) in quasi-phase-matched nonlinear media. Few-cycle pump pulses ($\lesssim$15 fs, 100 pJ) from a near-infrared electro-optic frequency comb are provided via nonlinear soliton-like compression in photonic-chip silicon-nitride waveguides. Subsequent intra-pulse DFG in periodically poled lithium niobate waveguides yields MIR frequency combs in the 3.1–4.8 μm region, while orientation-patterned gallium phosphide provides coverage across 7–11 μm. Cascaded second-order nonlinearities simultaneously provide access to the carrier–envelope-offset frequency of the pump source via in-line *f*-2*f* nonlinear interferometry. The high-repetition rate MIR frequency combs introduced here can be used for condensed phase spectroscopy and applications such as laser heterodyne radiometry.

https://doi.org/10.1364/OL.391651

Coherent broadband frequency comb sources in the mid-infrared (MIR, 3–25 μm) are valuable for studying light–matter interactions in molecular systems, e.g., trace-gas sensing and precision spectroscopy [1–4], time-resolved kinetics and dynamics of chemical reactions [5,6], and mapping the secondary structure of bio-molecular compounds [7,8]. Because only a few broad-bandwidth lasers directly emit radiation in the MIR [9–12], nonlinear frequency conversion is often employed to generate frequency combs in this spectral region [1,13]. Examples include difference frequency generation (DFG) [2,3,14–24], $\chi^{(2)}$ and $\chi^{(3)}$ parametric oscillators, as well as supercontinuum sources [25–28]. With intrapulse DFG, as we employ here, the broad spectrum of a near-infrared (NIR) pulse is downconverted to the MIR [9,29–33]. This is an attractive alternative to $\chi^{(2)}$ optical parametric oscillators or the more typical two-branch DFG, because it avoids the need for spatial and temporal overlap of multiple beams, and it provides broad simultaneous MIR spectral coverage. Recently, intrapulse DFG spectra from 3–12 μm have been demonstrated with combined brightness and bandwidth that is otherwise available only with a synchrotron light source [7,31,33,34].

Across these nonlinear techniques, most MIR frequency combs operate at rates on the order of 100 MHz due to the required nanojoule (or greater) pulse energies. For MIR spectroscopy of small gas-phase molecules at ambient temperatures and pressures, the ∼100 MHz comb mode spacing is a fraction of the typical linewidths. However, for larger gas-phase molecules and solid-state or liquid samples, the typical 100 MHz mode spacing is too fine, and sampling of a spectral resonance at 10 GHz (0.3 cm^{-1}) or greater would be more appropriate. Such large mode-spacing ($\geq$10 GHz) in the MIR is also highly desirable for applications such as imaging of biological materials [35–37] and spectroscopy of novel quantum materials [38] that demand fast acquisition rates ($\geq$1 MHz) and broad spectral coverage.

In this work, we generate broad-bandwidth and tunable MIR frequency combs at a rate of 10 GHz using common-place telecom-wavelength components and integrated photonics. We leverage a robust electro-optic (EO) comb generator [39] and $\chi^{(3)}$ spectral broadening in dispersion-engineered silicon nitride (Si_3N_4) waveguides to produce few-cycle NIR pulses. This source then drives intrapulse DFG [33] in quadratic nonlinear materials such as periodically poled lithium niobate (PPLN) waveguides and orientation-patterned gallium phosphide (OP-GaP). With this combination of techniques, devices, and materials, we overcome the challenging pulse energy limitations associated with high repetition rate sources to generate frequency combs across 3.1–4.8 μm and 7–11 μm. In this regime, a few MIR frequency comb systems have been explored with mode-spacings ranging from a few gigahertz [40,41] to 10 GHz and greater [42,43]. In comparison, our approach provides frequency combs with broader and more widely tunable bandwidth than existing quantum cascade laser (QCL) combs [11] and prior MIR EO frequency comb demonstrations [44,45]. At the same time, the 10 GHz mode-spacing enables applications such as dual-comb spectroscopy [46] over a 10 THz spectral window with a 10 MHz acquisition rate, which will be ideal for the hyper-spectral imaging of bio-chemical systems and real-time tracking of their dynamics.

We utilize a recently demonstrated EO frequency comb to generate few-cycle ($\lesssim$15 fs) pulses at 10 GHz in the NIR, centered at 1.55 μm [39]. The EO comb is generated via cascaded

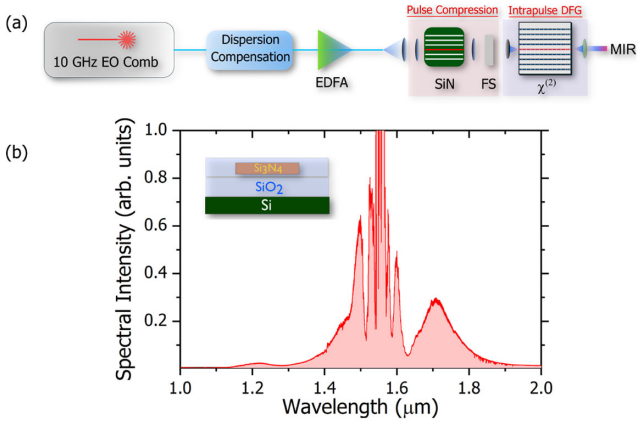

Fig. 1. Mid-IR electro-optic comb experimental setup. (a) Experimental setup for generating 10 GHz mid-infrared frequency combs. An electro-optic comb with 10 GHz repetition rate, centered at 1550 nm, is dispersion managed using a waveshaper and sent to an erbium-doped fiber amplifier (EDFA). Subsequent nonlinear spectral broadening in silicon nitride (SiN/Si_3N_4) nanophotonic waveguides results in few-cycle pulses that are approximately 15 fs in duration with 100 pJ of pulse energy. The few-cycle pulse drives intrapulse DFG in $\chi^{(2)}$ nonlinear media to generate mid-IR combs. (b) Corresponding spectrum of the few-cycle pulse. Inset: nanophotonic SiN waveguide geometry.

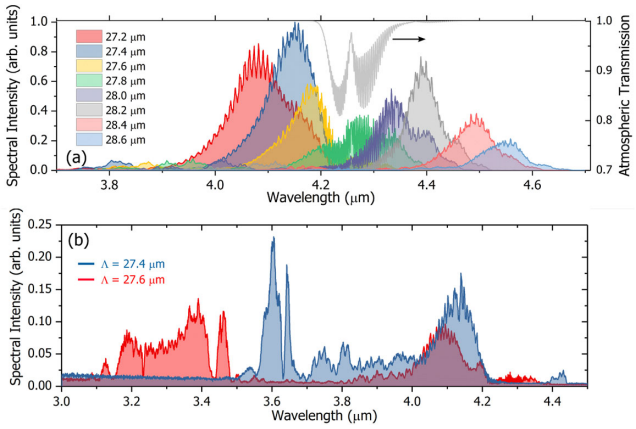

Fig. 2. Frequency comb generation from 3.1–4.8 μm. (a) Tunable MIR spectra are generated in 4-cm-long PPLN waveguides with various grating periods. Attenuation due to atmospheric carbon dioxide around 4.3 μm is observed over 2 m propagation. (b) By pre-chirping the few-cycle pump pulse using bulk fused silica windows (1 cm thick), broadband frequency conversion is observed in the waveguides.

phase and amplitude modulation {[39], Fig. 1(a)}. The output is amplified in an erbium-doped fiber amplifier to 4 W, spectrally broadened in 5-m-long normal group-velocity dispersion highly nonlinear fiber (ND-HNLF) with dispersion parameters $\beta_2 = 1.66\ \text{ps}^2/\text{km}$, $\beta_3 = 9.76 \times 10^{-3}\ \text{ps}^3/\text{km}$, and nonlinear coefficient $\gamma = 11/\text{W-km}$. The output of the ND-HNLF is compressed with free-space gratings to yield ~100 fs pulses. The ND-HNLF provides controlled spectral broadening that mitigates modulation instability, a common source of degradation of coherence in highly nonlinear spectral broadening processes. These pulses drive supercontinuum generation [Fig. 1(b)] in 2-cm-long Si_3N_4 waveguides (800 nm thickness, widths ranging from 1200 nm to 2000 nm, coupling efficiency ≈75%) that exhibit anomalous dispersion at 1.55 μm. Utilizing soliton self-compression in the waveguide [47], we generate few-cycle pulses with 1 W of average power, i.e., 100 pJ pulse energy, which are used to drive intrapulse DFG in PPLN or OP-GaP in the subsequent step.

In one configuration, we employ 4-cm-long PPLN ridge waveguides with poling periods spanning 25.6–30 μm to generate tunable, broadband combs from 3.8–4.6 μm via intra-pulse DFG using only 50 pJ of in-coupled pump-pulse energy [Fig. 2(a)]. The waveguides were fabricated by NTT Electronics America, by dicing Zn-doped PPLN waveguides on a lithium tantalate substrate [48]. The ridge dimensions are $12 \times 12\ \mu\text{m}^2$. The waveguide facets are anti-reflection coated for the pump wavelengths in the NIR. The pump light is in-coupled using an 11 mm focal length aspheric lens, and the waveguide output is collimated using a silver off-axis parabolic mirror. The input–output coupling efficiency is approximately 70% for the pump light in this configuration.

The center frequencies of the MIR output around 4.1 μm (≈73 THz) is understood by studying the spectral distribution of the pump [Fig. 1(b)]. The frequency difference between the two dominant peaks at the extrema, located at 1.2 μm (≈250 THz) and 1.7 μm (≈176 THz), yields 74 THz, which corresponds to 4.05 μm. We note that the 3-mm-thick Ge-substrate interference filters that transmit the MIR spectra form etalons and result in spectral modulation [Fig. 2(a)]. The powers in the MIR range from 50 μW for the output from the waveguide with $\Lambda = 28.6$ μm to 100 μW for the output from the waveguide with $\Lambda = 27.2$ μm. Utilizing a 1-cm-long fused silica (FS) window to optimize the pump-pulse compression, we also observed broad spectra spanning 3.1–4.3 μm that changed with the poling period [Fig. 2(b)]. The MIR output was spectrally isolated using germanium filters and directed to a Fourier-transform spectrometer (FTS) and a liquid nitrogen-cooled mercury-cadmium-telluride (MCT) photodetector for analysis. The integrated output power was between 50–100 μW, corresponding to >10 nW/nm spectral intensities.

The FTS can resolve individual comb lines in the MIR [Fig. 3(a)], showing that the nonlinear processes preserve the mode structure of the EO comb. However, the instrument resolution of 4 GHz artificially broadens the expected MHz-level comb tooth linewidths to the GHz level. As a result, we use a numerical model, which is a sum of Lorentzian lineshapes at a repetition rate of 10 GHz, to fit the data in Fig. 3(a). The model accounts for the finite resolution of the FTS and shows good agreement with the data. Moreover, the coherence of the comb in the NIR is manifest in the realization of an inline f-$2f$ interferometer in the PPLN waveguides.

Owing to the strong nonlinearity and phase-matched 2 μm to 1 μm second-harmonic generation (SHG) [49], the carrier–envelope offset frequency, f_{CEO}, of the comb is detected at 1 μm with >20 dB signal-to-noise ratio (SNR), as shown in the inset of Fig. 3(b). We note here that the f_{CEO} beat is strongly dependent on the output from the SiN waveguide as well as group-velocity matching in the 4-cm-long waveguide. In our experiment, the beat note can be observed in all the waveguides generating MIR light. Prior experiments have stabilized this degree of freedom in the EO comb [39], and the present experiment shows a simple route to its detection.

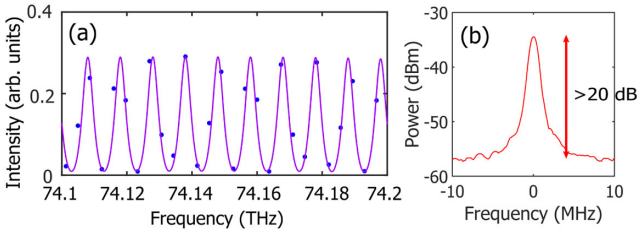

Fig. 3. 10 GHz modes in the mid-IR. (a) 10 GHz mode structure is observed in the mid-infrared around 74 THz (≈4.04 μm) as indicated by the blue dots and a fit (purple solid line). (b) The carrier–envelope offset frequency for the NIR EO comb is detected around 1.1 μm at the output of the 4-cm-long PPLN waveguide on a high-speed silicon photodetector, owing to in-line f-$2f$ interferometry. The detection frequency is around 3.5 GHz and the resolution bandwidth is 1 MHz.

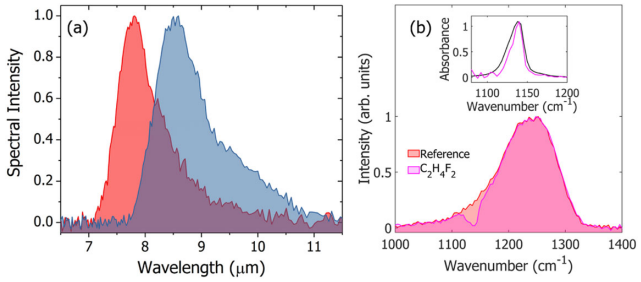

Fig. 4. 10 GHz frequency combs in the long-wave infrared. (a) LWIR spectra from OP-GaP pumped by few-cycle pulses from 1280 nm (red) and 1620 nm (blue) width Si_3N_4 waveguides. (b) Reference and transmission spectra for the measurement of $C_2H_4F_2$. Inset: measured absorption spectrum compared with the NIST WebBook database [50].

In addition to coherent sources in the 3–5 μm window, frequency combs in the molecular fingerprint region (6–20 μm) are of significant interest to the chemical, biological, and physical sciences [13,33]. Using the same intra-pulse DFG technique, we extend the spectral coverage from 7–11 μm using a 2-mm-long bulk, uncoated OP-GaP crystal with poling period $\Lambda = 60$ μm [Fig. 4(a)]. OP-GaP provides a large second-order nonlinear coefficient (≈35 pm/V) as well as a broad transparency (0.6–12 μm) into the long-wave infrared that is required for frequency comb generation in the molecular fingerprint region.

With 800 mW of input pump power, the measured output powers range from 70–100 μW. The output power of the OP-GaP was calibrated using the responsivity of the MCT photodetector at 7.5 μm and 8.5 μm, based on the average photocurrent measured. Accounting for the relatively high Fresnel losses at the crystal interface, we estimate that 300 μW could be generated. The integrated output power was calibrated using the MCT, and a 4 cm^{-1}-resolution FTS recorded the spectrum. For the FTS measurements, we collect a background spectrum with the MIR comb blocked and subtract it from the total spectrum with the comb incident. The residual pump light from the few-cycle driving pulse is filtered using a combination of 3-mm-thick germanium windows and longpass interference filters on germanium and silicon substrates. In contrast to the PPLN configuration, an inline f_{CEO} beat note is not observed due to the unfavorable phase-matching conditions in the OP-GaP crystal for the NIR. As a result, conventional f-$2f$ interferometry would be required to stabilize the carrier–envelope-offset frequency of the NIR frequency comb. The MIR output would still be offset-free in these conditions.

Although a single poling period was used in the OP-GaP, driving pulses from waveguides with widths 1280 nm and 1620 nm resulted in output spectra centered at 7.5 μm and 8.5 μm, respectively. The supercontinuum generation in the SiN waveguides with different widths provides a versatile method to optimize the pump-pulse spectrum compared to highly nonlinear fiber. In the OP-GaP, owing to the lower central frequencies in the long-wave infrared, the central peak of the pump at 1.55 μm (≈193.4 THz) participates in the nonlinear frequency conversion. Using the shorter-wavelength spectrum, we performed gas-phase spectroscopy of a commonplace refrigerant difluoroethane ($C_2H_4F_2$) from 1000−1400 cm^{-1} (7.1–10 μm), a spectral range that is 3–4 times broader than present QCL comb measurements [6]. The measured absorbance showed quantitative agreement with the NIST WebBook database spectrum {[50], Fig. 4(b), inset}.

In conclusion, we presented a robust technique to obtain broadband 10 GHz frequency combs in the MIR obtained using Er:fiber technology, electro-optics, and picojoule-scale nonlinear optics with integrated photonics platforms. Such sources should prove valuable for applications such as high-speed spectroscopy and imaging of large biological and chemical compounds. Furthermore, in place of the EO comb generator, recently developed solid-state 10-GHz-rate NIR frequency combs [51] can serve as efficient pump sources for the photonic-chip enabled nonlinear frequency conversion processes that would further simplify the experimental setup and provide robust performance. While state-of-the-art QCLs can provide much higher powers in the MIR, we anticipate that recent advances in nanophotonic lithium niobate [52] and gallium phosphide platforms [53] combined with careful pulse-shaping of the NIR driver [54,55] would further improve the frequency conversion efficiency into the MIR. Such powers can enable applications such as remote sensing using heterodyne interferometry [56].

Funding. Defense Advanced Research Projects Agency (SCOUT); Air Force Office of Scientific Research (FA9550-16-1-0016); National Institute of Standards and Technology.

Acknowledgment. We thank D. Lesko, N. Nader, and P. Acedo for helpful comments.

Disclosures. DRC is a co-founder of Octave Photonics, a company specializing in nonlinear integrated photonics. Certain commercial equipment, instruments, or materials are identified in this Letter to foster understanding. Such identification does not imply recommendation or endorsement by the National Institute of Standards and Technology, nor does it imply that the materials or equipment identified are necessarily the best available for the purpose.

REFERENCES

1. K. C. Cossel, E. M. Waxman, I. A. Finneran, G. A. Blake, J. Ye, and N. R. Newbury, J. Opt. Soc. Am. B **34**, 104 (2017).

2. G. Ycas, F. R. Giorgetta, E. Baumann, I. Coddington, D. Herman, S. A. Diddams, and N. R. Newbury, Nat. Photonics **12**, 202 (2018).
3. A. V. Muraviev, V. O. Smolski, Z. E. Loparo, and K. L. Vodopyanov, Nat. Photonics **12**, 209 (2018).
4. P. B. Changala, M. L. Weichman, K. F. Lee, M. E. Fermann, and J. Ye, Science **363**, 49 (2019).
5. A. J. Fleisher, B. J. Bjork, T. Q. Bui, K. C. Cossel, M. Okumura, and J. Ye, J. Phys. Chem. Lett. **5**, 2241 (2014).
6. J. L. Klocke, M. Mangold, P. Allmendinger, A. Hugi, M. Geiser, P. Jouy, J. Faist, and T. Kottke, Anal. Chem. **90**, 10494 (2018).
7. A. S. Kowligy, H. Timmers, A. J. Lind, U. Elu, F. C. Cruz, P. G. Schunemann, J. Biegert, and S. A. Diddams, Sci. Adv. **5**, eaaw8794 (2019).
8. M. L. Weichman, P. B. Changala, J. Ye, Z. Chen, M. Yan, and N. Picqué, J. Mol. Spectrosc. **355**, 66 (2019).
9. S. Vasilyev, I. Moskalev, V. Smolski, J. Peppers, M. Mirov, V. Fedorov, D. Martyshkin, S. Mirov, and V. Gapontsev, Optica **6**, 126 (2019).
10. S. Duval, M. Bernier, V. Fortin, J. Genest, M. Piché, and R. Vallée, Optica **2**, 623 (2015).
11. J. Faist, G. Villares, G. Scalari, M. Rosch, C. Bonzon, A. Hugi, and M. Beck, Nanophotonics **5**, 272 (2016).
12. S. Antipov, D. D. Hudson, A. Fuerbach, and S. D. Jackson, Optica **3**, 1373 (2016).
13. A. Schliesser, N. Picqué, and T. W. Hänsch, Nat. Photonics **6**, 440 (2012).
14. C. Erny, K. Moutzouris, J. Biegert, D. Kühlke, F. Adler, A. Leitenstorfer, and U. Keller, Opt. Lett. **32**, 1138 (2007).
15. A. Gambetta, R. Ramponi, and M. Marangoni, Opt. Lett. **33**, 2671 (2008).
16. A. Sell, R. Scheu, A. Leitenstorfer, and R. Huber, Appl. Phys. Lett. **93**, 251107 (2008).
17. F. C. Cruz, D. L. Maser, T. Johnson, G. Ycas, A. Klose, F. R. Giorgetta, I. Coddington, and S. A. Diddams, Opt. Express **23**, 26814 (2015).
18. F. Adler, K. C. Cossel, M. J. Thorpe, I. Hartl, M. E. Fermann, and J. Ye, Opt. Lett. **34**, 1330 (2009).
19. N. Leindecker, A. Marandi, R. L. Byer, and K. L. Vodopyanov, Opt. Express **19**, 6296 (2011).
20. A. Marandi, K. A. Ingold, M. Jankowski, and R. L. Byer, Optica **3**, 324 (2016).
21. M. Vainio and L. Halonen, Phys. Chem. Chem. Phys. **18**, 4266 (2016).
22. L. Maidment, O. Kara, P. G. Schunemann, J. Piper, K. McEwan, and D. T. Reid, Appl. Phys. B **124**, 143 (2018).
23. M. Yu, Y. Okawachi, A. G. Griffith, M. Lipson, and A. L. Gaeta, Optica **3**, 854 (2016).
24. C. Y. Wang, T. Herr, P. Del'Haye, A. Schliesser, J. Hofer, R. Holzwarth, T. W. Hänsch, N. Picqué, and T. J. Kippenberg, Nat. Commun. **4**, 2335 (2013).
25. C. R. Petersen, U. Møller, I. Kubat, B. Zhou, S. Dupont, J. Ramsay, T. Benson, S. Sujecki, N. Abdel-Moneim, Z. Tang, D. Furniss, A. Seddon, and O. Bang, Nat. Photonics **8**, 830 (2014).
26. B. Kuyken, S. Clemmen, S. K. Selvaraja, W. Bogaerts, D. V. Thourhout, P. Emplit, S. Massar, G. Roelkens, and R. Baets, Opt. Lett. **36**, 552 (2011).
27. D. D. Hudson, S. Antipov, L. Li, I. Alamgir, T. Hu, M. E. Amraoui, Y. Messaddeq, M. Rochette, S. D. Jackson, and A. Fuerbach, Optica **4**, 1163 (2017).
28. N. Nader, A. Kowligy, J. Chiles, E. J. Stanton, H. Timmers, A. J. Lind, F. C. Cruz, D. M. B. Lesko, K. A. Briggman, S. W. Nam, S. A. Diddams, and R. P. Mirin, Optica **6**, 1269 (2019).
29. R. Huber, A. Brodschelm, F. Tauser, and A. Leitenstorfer, Appl. Phys. Lett. **76**, 3191 (2000).
30. F. Keilmann, C. Gohle, and R. Holzwarth, Opt. Lett. **29**, 1542 (2004).
31. I. Pupeza, D. Sánchez, J. Zhang, N. Lilienfein, M. Seidel, N. Karpowicz, T. Paasch-Colberg, I. Znakovskaya, M. Pescher, W. Schweinberger, V. Pervak, E. Fill, O. Pronin, Z. Wei, F. Krausz, A. Apolonski, and J. Biegert, Nat. Photonics **9**, 721 (2015).
32. T. Butler, D. Gerz, C. Hofer, J. Xu, C. Gaida, T. Heuermann, M. Gebhardt, L. Vamos, W. Schweinberger, J. A. Gessner, T. Siefke, M. Heusinger, U. Zeitner, A. Apolonski, N. Karpowicz, J. Limpert, F. Krausz, and I. Pupeza, Opt. Lett. **44**, 1730 (2019).
33. H. Timmers, A. Kowligy, A. Lind, F. C. Cruz, N. Nader, M. Silfies, G. Ycas, T. K. Allison, P. G. Schunemann, S. B. Papp, and S. A. Diddams, Optica **5**, 727 (2018).
34. M. Seidel, X. Xiao, S. A. Hussain, G. Arisholm, A. Hartung, K. T. Zawilski, P. G. Schunemann, F. Habel, M. Trubetskov, V. Pervak, O. Pronin, and F. Krausz, Sci. Adv. **4**, eaaq1526 (2018).
35. H. Tu, Y. Liu, D. Turchinovich, M. Marjanovic, J. K. Lyngsø, J. Lægsgaard, E. J. Chaney, Y. Zhao, S. You, W. L. Wilson, B. Xu, M. Dantus, and S. A. Boppart, Nat. Photonics **10**, 534 (2016).
36. M. Hermes, R. B. Morrish, L. Huot, L. Meng, S. Junaid, J. Tomko, G. Lloyd, W. Masselink, P. Tidemand-Lichtenberg, C. Pedersen, F. Palombo, and N. Stone, J. Opt. **20**, 023002 (2018).
37. A. B. Seddon, B. Napier, I. Lindsay, S. Lamrini, P. M. Moselund, N. Stone, O. Bang, and M. Farries, Analyst **143**, 5874 (2018).
38. E. A. Muller, B. Pollard, H. A. Bechtel, R. Adato, D. Etezadi, H. Altug, and M. B. Raschke, ACS Photon. **5**, 3594 (2018).
39. D. R. Carlson, D. D. Hickstein, W. Zhang, A. J. Metcalf, F. Quinlan, S. A. Diddams, and S. B. Papp, Science **361**, 1358 (2018).
40. A. Mayer, C. Phillips, C. Langrock, A. Klenner, A. Johnson, K. Luke, Y. Okawachi, M. Lipson, A. Gaeta, M. Fejer, and U. Keller, Phys. Rev. Appl. **6**, 054009 (2016).
41. R. Rockmore, A. Laurain, J. V. Moloney, and R. J. Jones, Opt. Lett. **44**, 1797 (2019).
42. M. Yu, Y. Okawachi, A. G. Griffith, N. Picqué, M. Lipson, and A. L. Gaeta, Nat. Commun. **9**, 1869 (2018).
43. G. Scalari, J. Faist, and N. Picqué, Appl. Phys. Lett. **114**, 150401 (2019).
44. M. Yan, P.-L. Luo, K. Iwakuni, G. Millot, T. W. Hänsch, and N. Picqué, Light Sci. Appl. **6**, e17076 (2017).
45. B. Jerez, P. Martín-Mateos, F. Walla, C. de Dios, and P. Acedo, ACS Photon. **5**, 2348 (2018).
46. I. Coddington, N. Newbury, and W. Swann, Optica **3**, 414 (2016).
47. D. R. Carlson, P. Hutchison, D. D. Hickstein, and S. B. Papp, Opt. Express **27**, 37374 (2019).
48. M. Asobe, O. Tadanaga, T. Yanagawa, T. Umeki, Y. Nishida, and H. Suzuki, Electron. Lett. **44**, 288 (2008).
49. K. Iwakuni, S. Okubo, O. Tadanaga, H. Inaba, A. Onae, F.-L. Hong, and H. Sasada, Opt. Lett. **41**, 3980 (2016).
50. P. J. Linstrom and W. G. Mallard, *NIST Chemistry Webbook, NIST Standard Reference Database Number 69* (National Institute Standards Technology, 2020).
51. A. S. Mayer, C. R. Phillips, and U. Keller, Nat. Commun. **8**, 1673 (2017).
52. M. Jankowski, C. Langrock, B. Desiatov, A. Marandi, C. Wang, M. Zhang, C. R. Phillips, M. Lončar, and M. Fejer, Optica **7**, 40 (2020).
53. D. J. Wilson, K. Schneider, S. Hönl, M. Anderson, Y. Baumgartner, L. Czornomaz, T. J. Kippenberg, and P. Seidler, Nat. Photonics **14**, 57 (2020).
54. G. Campo, A. Leshem, F. Cappelli, I. Galli, P. C. Pastor, A. Arie, P. De Natale, and D. Mazzotti, J. Opt. Soc. Am. B **34**, 2287 (2017).
55. A. J. Lind, A. Kowligy, H. Timmers, F. C. Cruz, N. Nader, M. C. Silfies, T. K. Allison, and S. A. Diddams, Phys. Rev. Lett. **124**, 133904 (2020).
56. T. Kostiuk and M. J. Mumma, Appl. Opt. **22**, 2644 (1983).